Materials Research Bulletin 102 (2018) 36–44

Contents lists available at ScienceDirect

Materials Research Bulletin

journal homepage: www.elsevier.com/locate/matresbu

Study of the structural and magnetic phase-transitions and multiferroic properties in $BiFeO_3$-$Ba_{0.95}Ca_{0.05}TiO_3$ solid solutions

Jaswinder Pal, Sunil Kumar, Lakhwant Singh, Mandeep Singh, Anupinder Singh*

Multifunctional Materials Laboratory, Department of Physics, Guru Nanak Dev University, Amritsar, Punjab, 143005, India

ARTICLE INFO

Keywords:
Multiferroics
Ferroelectrics
Dielectric
Magnetism
Ceramics
$BiFeO_3$

ABSTRACT

We synthesized (1-x) $BiFeO_3$-x $Ba_{0.95}Ca_{0.05}TiO_3$ solid solutions for $0.1 \leq x \leq 0.9$, using a solid-state-reaction. The XRD analysis reveals that a composition-driven rhombohedral-to-cubic and a cubic-to-tetragonal phase-transition occur at $x \approx 0.4$ and $x \approx 0.7$, respectively. The experiments show that $BaCaTiO_3$-substitution suppresses the spiral spin-structure, which leads to net magnetization. The samples have been found to exhibit magnetic order for $0.1 \leq x \leq 0.7$ and paramagnetic behavior for $x \geq 0.8$. The electrical conductivity increases with increasing frequency of the applied electric field. The dielectric measurements suggest a non-Debye type relaxation. The samples show magneto-dielectric response (MD) upto $x = 0.5$, with the highest MD of 11.61% at 10 kHz for $x = 0.3$. The maximum attainable remanent polarization (P_r) ~ 5.24 μC/cm^2 was observed for $x = 0.7$.

1. Introduction

There is increasing interest in material research to find materials with more than one ferroic property. Such materials are known as magnetoelectric or multiferroic materials [1]. Because these materials exhibit magnetoelectric effects, it is possible to control their magnetization through an external electric field and vice-versa [2,3]. This property of controlling magnetization through an electric field and polarization via a magnetic field renders multiferroic materials useful for applications such as sensors, spintronic devices, memory devices, piezoelectric actuators, and microelectromechanical systems [4–8]. Unfortunately, achieving ferromagnetic and ferroelectric order in a single phase is challenging due to opposing requirements for the electronic configuration of transition metal ions (the d°- d^n problem) [9]. The multiferrocity is generally observed in perovskite ceramics with the general formula ABO_3, where the A-site is occupied by a large cation and the B-site is occupied by a smaller cation. The resulting distortions and orientations by cations in perovskites generate materials with a wide range of properties, which are studied to understand the facilitation of multifunctionality [10].

$BiFeO_3$ (BF) is a magnetoelectric material with an antiferromagnetic Neel-temperature (T_N) of about 350–370 °C, and a ferroelectric Curie-temperature (T_C) of about 810–830 ° C [11]. However, high leakage currents, very weak magnetoelectric coupling, and a cycloidal spin structure limit the utility of BF for practical applications [12,13]. Various approaches are used worldwide to improve the performance of BF-based multiferroic materials. In recent years, mixed perovskites have been successfully synthesized. Kumar et al. reported the synthesis of (1-x) $BiFeO_3$-x $BaTiO_3$ solid solutions for $0.1 < x < 0.3$, using a conventional solid-state reaction-route [14]. They observed that doping a small amount of **$BaTiO_3$ (BT)** into BF causes the release of latent magnetization, which was previously locked up within the spiral spin structure. Anar Singh et al. found evidence for composition-driven rhombohedral-to-cubic and cubic-to-tetragonal morphotropic phase-transitions in (1-x) $BiFeO_3$-x $BaTiO_3$ solid solutions at $x = 0.35$ and 0.85, respectively [15]. Wang et al. used $CaTiO_3$ to modify the multiferroic properties of BF [16]. They reported that single-phase $(Bi_{1-x}Ca_x)(Fe_{1-x}Ti_x)O_3$ solid solutions ($x \geq 0.15$) show increased dielectric constants and magnetization, lower leakage-currents, and dielectric loss. Barium calcium titanate (BCT) is another class of perovskite materials, which is one of the most promising candidates for practical applications thanks to its high dielectric constant, low leakage-current, tunable Curie temperature, and high piezoelectric/electrostrictive properties. However, weak magnetoelectric-coupling and phase impurities limit the use of BCT for practical applications [17,18].

Thus, we believe that enhancement of the magnetoelectric effect and the ferroic properties could be achieved by forming solid solutions of BF with other perovskites. In our view, BCT is a promising candidate to obtain a solid solution with BF. In addition, a solid solution of BF with BCT has not yet been studied, to the best of our knowledge. Therefore, we have chosen to. In this paper, we report the synthesis of (1-x) $BiFeO_3$- x $Ba_{0.95}Ca_{0.05}TiO_3$ binary solid solution with compositions ranging from $x = 0.1$ to $x = 0.9$,

* Corresponding author.
E-mail address: anupinders@gmail.com (A. Singh).

https://doi.org/10.1016/j.materresbull.2018.02.012
Received 28 May 2017; Received in revised form 5 January 2018; Accepted 5 February 2018
Available online 07 February 2018

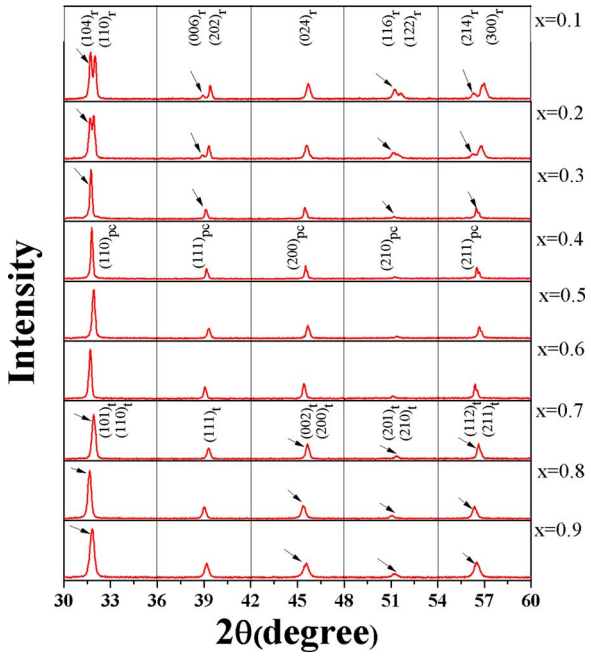

Fig. 1. The XRD raw data of (1-*x*) BF-*x* BCT ($0.1 \le x \le 0.9$) samples.

using a conventional solid-state reaction route. We also study the resulting solid solution with respect to their structural, dielectric, ferroelectric, magnetic, magnetodielectric, and electric properties.

2. Experimental

The (1-*x*) BF- *x* BCT ($0.1 \le x \le 0.9$) ceramic solid solutions were prepared using a conventional solid-state reaction route. Bi_2O_3, Fe_2O_3, $BaCO_3$, $CaCO_3$, and TiO_2 (99.9% purity, obtained from Sigma Aldrich) were used as starting materials. The stoichiometrically weighted binary powders were mixed using a pestle and mortar for one hour. This mixed powder was transferred to a bottle containing propanol and zirconia balls, then ball-milled successively for 24 h and 12 h using a simple and a planetary ball mill, respectively. The milled powder was dried and calcined in a high-temperature furnace for 12 h. The calcination was performed at 900 °C and 1000 ºC for $0.1 \le x \le 0.3$ and $0.4 \le x \le 0.9$, respectively. The calcined powder was then mixed with poly vinyl alcohol (PVA) binder (2 wt %). The resulting powder was pressed to obtain pellets of 10 mm diameter and thickness ~1 mm, using a hydraulic press. The resulting pellets were sintered for 2 h. Sintering was performed at 1050 ºC for $0.1 \le x \le 0.3$, and at 1200 ºC for $0.4 \le x \le 0.9$. The room temperature XRD data of the sintered samples were recorded between 10° and 120° with a step size of 0.02° and a scan speed of 2°/min, using a Shimadzu diffractometer (Maxima) equipped with a Cu Kα (λ = 1.54 Aº) anode. The **Le Bail** refinement of the XRD data was carried out using the software Fullprof [19]. The surface morphology was investigated with a FE-SEM (Supra 55) from Carl Zeiss, and energy-dispersive X-ray analysis (EDX) **X-Max 51-XMX0004 from Oxford Instruments** was used to determine the chemical composition of the samples. Magnetization hysteresis (M-H) measurements were carried out at room temperature with a vibrating sample magnetometer (VSM) EZ-9 from Microsense. The dielectric studies were done with an impedance analyzer (Keysight-E4990A). The ferroelectric properties were measured with an automatic PE loop tracer from Marine India.

3. Results and discussion

3.1. XRD analysis

Fig. 1 shows the room temperature X-ray diffractogram for (1-*x*) BF-*x* BCT ($0.1 \le x \le 0.9$). The reflections at 2θ of about 31.72°, 39.11°, 51.20°, and 56.50° are doublets for $x < 0.3$ and singlets for $0.4 \le x \le 0.6$. For $x = 0.3$, the peaks are only asymmetrically broadened, and peak splitting is not visible to the naked eye. For $x > 0.6$ the reflections are again asymmetrically broadened. The presence of doublet peaks for $x \le 0.3$ suggests a crystal structure of lower symmetry. The absence of doublet peaks for $0.4 \le x \le 0.6$ indicates the presence of a crystal structure of higher symmetry. The asymmetric broadening for $x > 0.6$ confirms the presence of a crystal structure of lower symmetry. Thus, we expect that for $x \le 0.3$, the crystal structure should be similar to BF (Rhombohedral, R3c space group), while for $0.4 \le x \le 0.6$ the crystal structure should be closer to simple cubic (Pm-3 m space group), and for $x > 0.6$ the crystal structure should be similar to BCT (tetragonal, P4mm).

Fig. 2 shows the observed, calculated, and difference data obtained using the **Le Bail** analysis of the XRD data for $0.1 \le x \le 0.9$. The **Le Bail** analysis was carried out using the R3c space group for $x \le 0.3$, the Pm-3m space group for $0.4 \le x \le 0.6$, and the P4mm space group for $x \ge 0.7$. For samples with $x \le 0.3$, we calculated the lattice parameters of the equivalent elementary rhombohedral cell ("a" and "c") using hexagonal cell parameters ("a_h" and "c_h"). The equivalent elementary rhombohedral lattice parameters are related to hexagonal lattice parameters via $a \approx a_H/\sqrt{2}$ and $c \approx c_H/2\sqrt{3}$ [15]. The refined lattice parameters, c/a ratio, goodness of fit (GOF) and cell volume, calculated from **Le Bail** refinements for all compositions, is summarized in Table 1. Fig. 3(a–c) shows the variation of lattice parameters, c/a ratio, and cell volume as a function of composition (*x*). Fig. 3(a) shows that the lattice parameter "a" and "c" have unequal values for $x \le 0.3$ and $x \ge 0.7$ but equal values for $0.4 \le x \le 0.6$. In other words, the samples possess rhombohedral symmetry for $x \le 0.3$, cubic symmetry for $0.4 \le x \le 0.6$, and tetragonal symmetry for $x \ge 0.7$. Fig. 3 (b) shows that the c/a ratio reaches a maximum at $x = 0.1$ and starts decreasing with increasing *x* (until $x = 0.3$). This decrease suggests a reduction in the rhombohedral distortion. For $0.4 \le x \le$n0.6, the c/a ratio remains constant, which means that the system has cubical symmetry. The c/a ratio again starts to increase slightly between $x = 0.7$ and $x = 0.9$, which indicates a weak tetragonal distortion. Hence it is clear that a rhombohedral to cubic transformation takes place between $x = 0.3$ and $x = 0.4$, while a cubic to tetragonal transformation takes occurs between $x = 0.6$ and $x = 0.7$. Fig. 3(c) reveals that the cell volume increases rapidly until $x = 0.3$ and much slower after $x = 0.4$. For $x \ge 0.7$, the cell volume is almost constant. Anar Singh et al. [15] also reported a composition-driven rhombohedral to cubic and cubic to tetragonal phase-transition in (1-*x*) BF-*x* BT solid solutions at $x = 0.35$ and 0.85, respectively.

3.2. SEM and EDX

Fig. 4 shows the scanning electron microscope (SEM) micrographs of (1-*x*) BF- *x* BCT for $0.1 \le x \le 0.9$. All samples show small, homogenous, randomly oriented, well-interlinked, and non-uniform grains (with respect to shape and size). The average grain size decreases from 7.25 μm to 0.31 μm as *x* increases from 0.1 to 0.9. The average grain-size also decreases with increasing BCT content (between $x = 0.1$ and $x = 0.9$). Fig. 5 shows the energy dispersive X-ray analysis (EDX) spectra of 0.9BF- 0.1BCT ceramics. The figure indicates that the prepared 0.9BF- 0.1BCT ceramics contain only Bi, Ba, Ca, Fe, Ti, and O. No other elemental impurities were detected. The elemental composition, as determined from the EDX spectra, matches the stoichiometric composition. Similar results were obtained for other compositions ($0.2 \le x \le 0.9$).

3.3. Magnetic characterization at room temperature

The magnetization versus magnetic field (M-H) hysteresis loops for (1-*x*) BF-*x* BCT ($0.1 \le x \le 0.9$) ceramics were recorded at room